







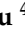






## Article

# Photodiode Read-Out System for the Calorimeter of the Herd Experiment

Pietro Betti <sup>1,2,\*</sup>, Oscar Adriani <sup>1,2</sup>, Matias Antonelli <sup>3</sup>, Yonglin Bai <sup>4</sup>, Xiaohong Bai <sup>4</sup>, Tianwei Bao <sup>4</sup>, Eugenio Berti <sup>1,2</sup>, Lorenzo Bonechi <sup>2</sup>, Massimo Bonghi <sup>1,2</sup>, Valter Bonvicini <sup>3</sup>, Sergio Bottai <sup>2</sup>, Weiwei Cao <sup>4</sup>, Jorge Casaus <sup>5</sup>, Zhen Chen <sup>4</sup>, Xingzhu Cui <sup>4</sup>, Raffaello D'Alessandro <sup>1,2</sup>, Sebastiano Detti <sup>2</sup>, Yongwei Dong <sup>4</sup>, Noemi Finetti <sup>2,6</sup>, Valerio Formato <sup>7</sup>, Miguel Angel Velasco Frutos <sup>5</sup>, Jiarui Gao <sup>4</sup>, Xiaozhen Liang <sup>4</sup>, Ran Li <sup>4</sup>, Xin Liu <sup>4</sup>, Linwei Lyu <sup>4</sup>, Gustavo Martinez <sup>5</sup>, Nicola Mori <sup>2</sup>, Jesus Marin Munoz <sup>5</sup>, Lorenzo Pacini <sup>2</sup>, Paolo Papini <sup>2</sup>, Cecilia Pizzolotto <sup>3</sup>, Zheng Quan <sup>4</sup>, JunJun Qin <sup>4</sup>, Dalian Shi <sup>4</sup>, Oleksandr Starodubtsev <sup>2</sup>, Zhicheng Tang <sup>4</sup>, Alessio Tiberio <sup>2</sup>, Valerio Vagelli <sup>8,9</sup>, Elena Vannuccini <sup>2</sup>, Bo Wang <sup>4</sup>, Junjing Wang <sup>4</sup>, Le Wang <sup>4</sup>, Ruijie Wang <sup>4</sup>, Gianluigi Zampa <sup>3</sup>, Nicola Zampa <sup>3</sup>, Zhigang Wang <sup>4</sup>, Ming Xu <sup>4</sup>, Li Zhang <sup>4</sup> and Jinkun Zheng <sup>4</sup>

<sup>1</sup> Dipartimento di Fisica e Astronomia, Università degli Studi di Firenze, 50019 Sesto Fiorentino, Italy

<sup>2</sup> INFN Firenze, 50019 Sesto Fiorentino, Italy

<sup>3</sup> INFN Trieste, 34149 Trieste, Italy

<sup>4</sup> Chinese Academy of Sciences, Beijing 100049, China

<sup>5</sup> CIEMAT, 28040 Madrid, Spain

<sup>6</sup> Dipartimento di Scienze Fisiche e Chimiche, Università degli Studi dell'Aquila, 67100 L'Aquila, Italy

<sup>7</sup> INFN—Sezione di Roma Tor Vergata, 00133 Roma, Italy

<sup>8</sup> Agenzia Spaziale Italiana, 00133 Roma, Italy

<sup>9</sup> INFN Perugia, 06100 Perugia, Italy

\* Correspondence: betti@fi.infn.it



**Citation:** Betti, P.; Adriani, O.; Antonelli, M.; Bai, Y.; Bai, X.; Bao, T.; Berti, E.; Bonechi, L.; Bonghi, M.; Bonvicini, V.; et al. Photodiode Read-Out System for the Calorimeter of the Herd Experiment. *Instruments* **2022**, *6*, 33. <https://doi.org/10.3390/instruments6030033>

Academic Editors: Fabrizio Salvatore, Alessandro Cerri, Antonella De Santo and Iacopo Vivarelli

Received: 30 July 2022

Accepted: 31 August 2022

Published: 2 September 2022

**Publisher's Note:** MDPI stays neutral with regard to jurisdictional claims in published maps and institutional affiliations.



**Copyright:** © 2022 by the authors. Licensee MDPI, Basel, Switzerland. This article is an open access article distributed under the terms and conditions of the Creative Commons Attribution (CC BY) license (<https://creativecommons.org/licenses/by/4.0/>).

**Abstract:** HERD is a future experiment for the direct detection of high energy cosmic rays. The instrument is based on a calorimeter optimized not only for a good energy resolution but also for a large acceptance. Each crystal composing the calorimeter is equipped with two read-out systems: one based on wavelength-shifting fibers and the other based on two photodiodes with different active areas assembled in a monolithic package. In this paper, we describe the photodiode read-out system, focusing on experimental requirements, design and estimated performances. Finally, we show how these features lead to the flight model project of the photodiode read-out system.

**Keywords:** cosmic rays; calorimeters; space instrumentation; large detector systems for particle and astroparticle physics

## 1. Introduction

The direct measurements of high-energy cosmic rays are limited by the geometrical acceptance of space experiments, since at high energy the flux is described by a power law  $J^{-\gamma}$  with a spectral index  $\gamma$  of about 2.7, strongly limiting the number of particles at these energies. The HERD (*High Energy cosmic-Radiation Detector*) [1,2] experiment is a new direct experiment planned to be installed on the *Chinese Space Station* in 2027, whose aim is to improve and extend the current measurements at high energies. Indeed, the experiment has been designed in order to directly measure protons and nuclei up to the cosmic ray *knee* region at about 1 PeV, and *electron+positron* flux up to tens of TeV, at least one order of magnitude higher than the current experiments. In addition, HERD will also detect high-energy photons in order to look for cosmic ray sources. Furthermore, both measurements of *electron+positron* flux and high energy photons are a valuable tool in searching for indirect evidence of dark matter.

The main component of the HERD detector is a homogeneous, isotropic, 3-D, finely segmented and deep (about 55  $X_0$  and 3  $\lambda_1$ ) calorimeter. As shown on the left side of

Figure 1, the calorimeter will be composed of about 7500 LYSO cubic scintillating crystals (with a side of 3 cm) assembled in an octagonal-based prism.

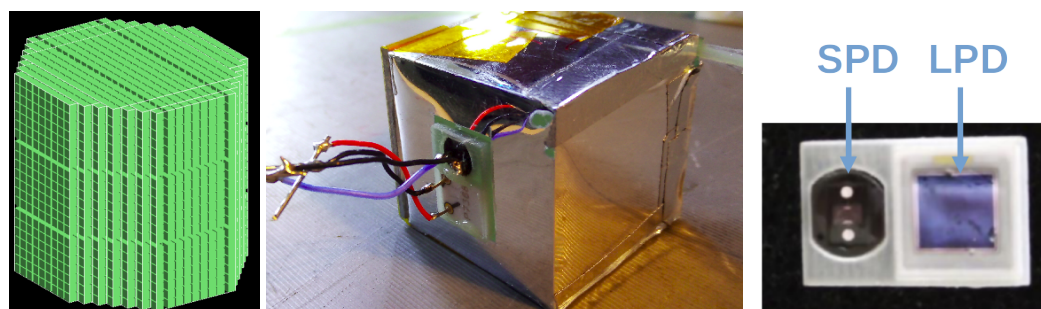


**Figure 1.** On the left: scheme of the structure of the calorimeter, about 7500 LYSO cubic crystals are assembled in an octagonal-based prism. In the center: picture of a LYSO crystal with WLSF and PD read-out systems installed; the crystal is covered with a reflective coating. On the front side of the crystal a monolithic package with photodiodes is glued to the crystal. The WLSFs are glued on the top face of the crystal, but are covered by the reflective coating; however, we can see the fibers coming outside of the reflective coating in the upper right corner of the image. On the right: an illustration of an in-house-built prototype of a monolithic package for the PD read-out system.

Each crystal of the calorimeter is equipped with two different read-out systems: one based on *Wave Length Shifting Fibers* (WLSF) coupled with Intensified scientific CMOS cameras, the other one based on the use of two photodiodes with different active areas (PD system). A picture of a crystal equipped with both read-out systems is shown in the central panel of Figure 1. The use of two independent read-out systems is very important in order to have strong control on the energy scale (two independent calibrations), two independent triggers and redundancy. In this proceeding, the system requirements, the design and the performances of the PD system are analyzed. Before going on, we briefly describe the WLSF read-out system in order to give the reader a general view of the read-out system alternative to the PD system. The WLSF read-out system consists of two fibers (with a diameter of 300  $\mu\text{m}$  each) for each crystal, that collect light and then emit it at their extremities in the green wavelength region. The fibers are connected via a thin optical guide to a surface of the crystal in order to collect LYSO scintillating photons. One extremity of each fiber is connected to a CMOS camera: one high-gain CMOS and one low-gain CMOS. The use of two CMOS with different gains is necessary in order to reach a very high dynamic range. In addition, the remaining extremities of the fibers are connected to photomultiplier tubes that collect and sum signals from different crystals in order to provide fast information on the energy deposit in a certain region of the calorimeter that can be used for trigger purposes.

The HERD calorimeter is surrounded by other subdetectors for tracking, charge measurement and anticoincidence purposes. In this way, HERD is able to detect particles entering the detector not only from the zenith but also from the lateral sides. This design, together with the calorimeter features, achieves an acceptance which is about three times larger than that of typical calorimeters with the same volume and mass, as was demonstrated by the CaloCube collaboration [3–8]. Indeed, HERD will have an effective geometric factor (convolution of geometric acceptance and detection efficiency) about one order of magnitude larger than that of current space experiments: about 2–3  $\text{m}^2\text{sr}$  for electrons and about 1  $\text{m}^2\text{sr}$  for protons, instead of the 0.3  $\text{m}^2\text{sr}$  and 0.1  $\text{m}^2\text{sr}$  of DAMPE experiment [9], the largest effective geometric factors of currently in-orbit experiments. This is a key factor for extending cosmic rays fluxes measurements at higher energies.

## 2. Design of the Photodiode Read-Out System

The main requirements for both WLSF and PD systems are low power consumption and an exceptionally large dynamic range. The first is constrained by the limited power availability on the space station, while the second is necessary to measure the deposit by

high energy showers and, at the same time, to calibrate the detector with MIP (*minimum ionizing particles*) protons and nuclei. Indeed simulations show that a shower induced by a PeV proton can release up to 250 TeV in a single crystal. On the other hand, in-flight calibration with MIPs requires measuring energy deposits of about 30 MeV, i.e., the energy deposit of a minimum ionizing proton in a 3 cm LYSO cube. Thus, a very high dynamic range of about  $10^7$  is needed for the read-out systems.

The PD system is based on pairs of photodiodes with different active areas: the large photodiode (LPD, model VTH2110 produced by Excelitas) and the small photodiode (SPD, model VTP9412 produced by Excelitas) with active areas, respectively, of 25 mm<sup>2</sup> and 1.6 mm<sup>2</sup>. LPD and SPD are assembled in a custom monolithic package, as shown in the right panel of Figure 1 (a new monolithic package developed with Excelitas is currently under production as we will show in Section 5). Using two photodiodes with different active areas allows for an increase in the dynamic range: LPD can detect signals smaller than the SPD thanks to the larger active area, while the SPD signals saturate the front-end electronics at higher energies than LPD ones. Multiple measurements of the ratio between LPD and SPD gains at different test beams will be discussed in the next sections.

To satisfy the requirements on power consumption, noise and dynamic range, a dedicated front-end chip has been developed specifically for this system. This chip is called HiDRA2, based on the CASIS ASIC [10], and is the principal component of the front-end-electronics (FEE) for the PD system. The main characteristics of this chip are: a low power consumption of about 3.75 mW per channel, a low noise with an *Equivalent Noise Charge* (ENC) of about 2500 *equivalent electrons* and a high dynamic range from few fC to 52.6 pC. The single read-out channel of the HiDRA2 chip is composed of two main parts: a *Charge Sensitive Amplifier* (CSA) followed by a *Correlated Double Sampling* (CDS). The CSA has two different gains. The gain is automatically selected for each channel on an event-by-event basis; this allows it to reach a high dynamic range of the FEE without doubling the number of channels. The ratio between *high-gain* and *low-gain* is about 20, and laboratory measurements show that the uncertainty on this value is smaller than 1%.

Photodiodes are connected to the FEE via specifically designed Kapton cables. Every cable can simultaneously connect up to 10 crystals (10 LPD-SPD couples) and is long about 26 cm. In the flight model Kapton cables will be longer and will connect up to 21 crystals. A long Kapton cable extension (about 68 cm) has been produced in order to extend the length of the current one and was used to estimate the noise for the flight model.

### 3. Performance of the Photodiode Read-Out System

In this section, we show the main performances of the PD read-out system measured with several laboratory tests and test beams. In particular, we will focus on the noise of the system, the measurement of cosmic muon MIP, and the ratio between LPD and SPD gains. The noise of the system was estimated using the standard deviation of the Gaussian fit performed on the pedestal distribution. These measurements were performed in two different configurations: with the normal Kapton cable (as shown in the left peak of Figure 2 left panel) and with the addition of the Kapton extension to simulate the flight model length.

Furthermore, the noise was measured connecting photodiodes of several instrumented crystals: the typical noise values were about 22.5 *ADC channels* without the extension and 27.5 *ADC* with the extension. Hence, in the flight model, an increase of noise of at least 20% with respect to the current configuration is expected due to the longer cables.

The energy released by an MIP is the minimum signal that we want to be able to detect in a single crystal. We measured the typical MIP distribution by using cosmic muons, as shown in the right peak of Figure 2 central panel for an LPD. LPD muon signal distributions were fitted with the convolution of Gaussian and Landau distributions, while for SPD signal distributions simple Gaussian distributions were used since the MIP values for SPD were very small and the noise dominated the signal. MIP measurements were performed with a few crystals. From these measurements we determined an average

$MIP_{LPD} = (110 \pm 10) \text{ ADC}$ , and  $MIP_{SPD} = (6 \pm 2) \text{ ADC}$ . Even considering a noise of about 30 ADC (larger than the measured one due to possible degradation in the final detector) the *Signal to Noise Ratio* is expected to be  $SNR_{LPD} > 3.5$ , while  $SNR_{SPD} < 1$ . Thus, LPD can be calibrated with MIP signals, whereas SPD can be calibrated by exploiting the correlation with LPD.

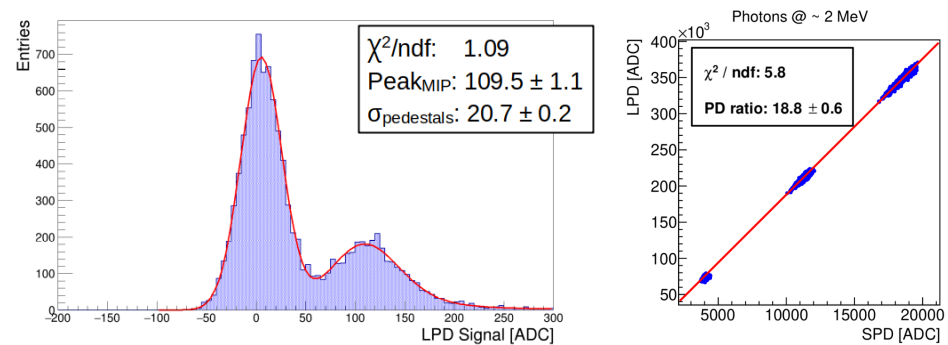


**Figure 2.** Left panel: MIP distribution of a LPD; the left peak is the pedestal peak while the one on the right is the MIP events peak. Right panel: correlation plot between LPD and SPD measured with a multiparticle beam of photons with a mean energy of 2 MeV.

The LPD/SPD gain ratio was measured at two test beams with multiparticle beams of 2 MeV protons at the Labec facility [11] and photons with a mean energy of 2 MeV with a medical radiotherapy accelerator. In particular, beam multiplicities were varied in order to scan a sufficiently large region of the dynamic range of the system. Then, correlation plots between LPD and SPD signals were built and a linear fit was performed. The angular coefficient resulting from the fit was the ratio between LPD and SPD gains. This is shown in Figure 2 right for one of the few crystals tested. The resulting average LPD/SPD gain ratio was  $19.0 \pm 1.5$ . Further measurements with different beams are foreseen to extend the range of the energy scan and confirm these values.

#### 4. Calibration of the Prototype Tested at Sps

After developing and testing the sensor system for a single crystal, a prototype of the calorimeter was assembled. The prototype was composed of 525 crystals all equipped with WLSE, with only 63 of them equipped with photodiodes due to mechanical and procurement constraints. The prototype was tested at the CERN SPS in October 2021. In this section, we show the calibration procedure of the PD system of the prototype as it was performed with the data acquired at the test beam; other results of the ongoing analysis will be the subject of a forthcoming paper.

The noise was estimated as in the previous section, performing Gaussian fits on pedestal histograms. The noise mean value was about 18.5 ADC. This value was lower than the one measured in laboratory tests (shown in Section 3).

LPDs were calibrated by measuring energy releases of MIP. In this case, a muon beam with energy of 250 GeV was used. A typical histogram for MIP signals is shown on the left side of Figure 3.

The distribution showed two peaks: the right peak was the main peak of MIP signals and was fitted with the convolution of Gaussian and Landau distributions. The left peak was due to triggered events in which the beam did not hit the crystal (i.e., pedestal events) and was fitted with a Gaussian distribution. As we can see, the pedestal distribution was not centered on zero because of a baseline recovery problem in case of high energy release. Thus, the simultaneous fit of the two peaks was important to properly estimate the energy deposit. This problem is currently being solved thanks to a firmware and electronic update, and it will not be present in future tests. The mean value of the MIP for 250 GeV muons for all crystals was equal to  $(126 \pm 4) \text{ ADC}$ . This value was slightly larger than that measured with cosmic muons. This was mainly due to the different energy of the muons considered,

indeed cosmic muons have an energy distribution centered at a few GeV, while muons at the test beam had 250 GeV energy.

Then the ratio between LPD and SPD gains has been measured with a correlation plot and linear fit, in the same way, that was described in the previous section. A correlation plot for a crystal is shown on the right side of Figure 3. Considering all the crystals, the mean value of the LPD/SPD gain ratio was equal to  $18.7 \pm 0.9$ , compatible with the value reported in the previous section. In the next section, these parameters will be used to determine the dynamic range of the PD read-out system.

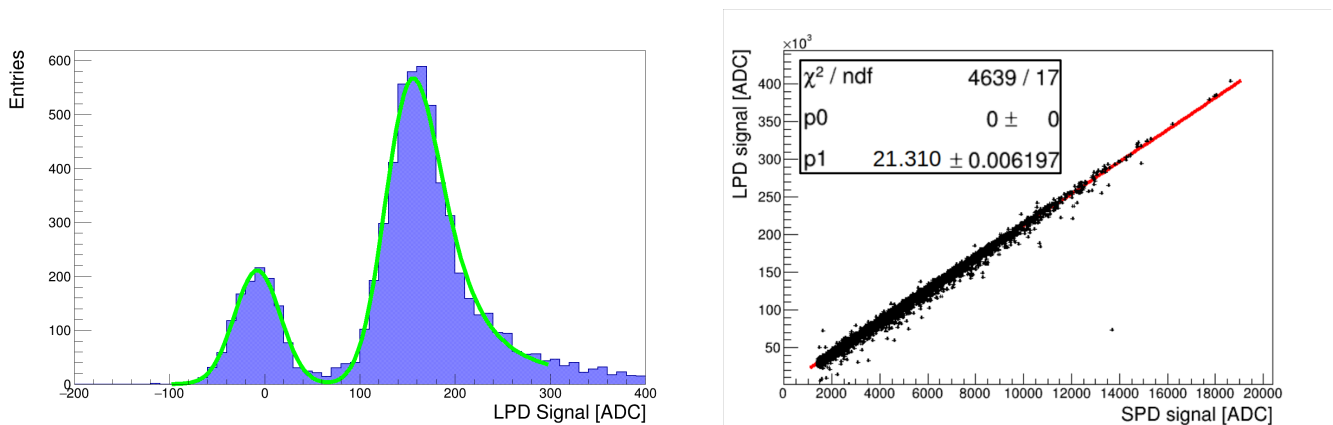


**Figure 3.** (Left side): MIP distribution of an LPD. (Right side): correlation plot between LPD and SPD signals for a crystal.

### 5. Results

In the previous section, the MIP values and LPD/SPD gain ratio values for multiple crystals have been measured. In addition, from simulations, we know that the muon MIP releases are about 30 MeV in the single crystal. From the saturation level of the HiDRA2 chip it is possible to estimate the saturation levels for LPD and SPD: about 190 GeV for LPD and 3.5 TeV for SPD. However, the system should be able to measure up to 250 TeV energy releases in a single crystal, thus the SPD input signal should be attenuated in order to shift the saturation level to higher energies. In doing this we must be careful in keeping an overlapping region between the operative ranges of LPD and SPD since their correlation is the only possible method to calibrate the SPD gain.

It has been decided to cover the SPD surface with an optical filter with a transmittance of 1.5%. In this way, the new saturation level is about 250 TeV, while the SNR of SPD at the LPD saturation level is bigger than 15, which permits the SPD calibration. In Figure 4 a scheme of the dynamic range of the system with both normal and optically filtered SPD is shown.

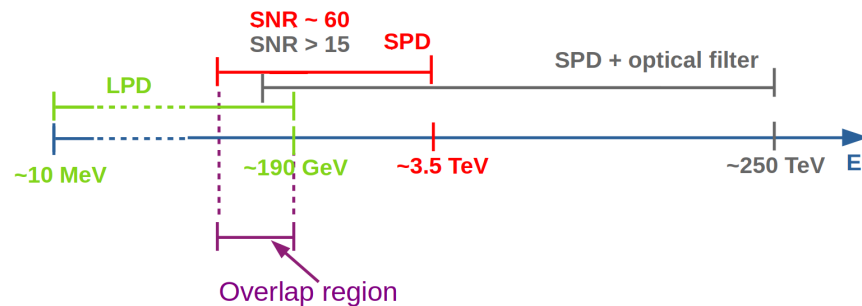


**Figure 4.** Scheme of the dynamic range of the system. The absolute energy scale is depicted in blue, the LPD dynamic range in green, the SPD dynamic range in red, the SPD optically filtered dynamic range in grey, and the overlapping region between LPD and SPD in purple.

The new project of the monolithic package with the optical filter on the SPD surface has already been developed in collaboration with Excelitas. The new packages are in production and the first 1000 packages will be ready at the beginning of 2023. They will be characterized and mounted in a new calorimeter prototype of 1000 crystals, that will be tested at SPS at the end of 2023.

## 6. Discussion

In this paper, we have shown the developments and the tests of the photodiode read-out system of the calorimeter of the HERD experiment. The performances of the system and the developments of the monolithic package for the flight model, which is now under production, have been illustrated. Finally, it is planned to equip a new calorimeter prototype with 1000 new monolithic packages and to test it at SPS at the end of 2023.

**Author Contributions:** Conceptualization, O.A., R.D. and J.C.; methodology, P.B., E.B., L.P.; software, P.B., E.B., L.P. and A.T.; validation, P.B., E.B. and L.P.; formal analysis, P.B., E.B. and L.P.; investigation, O.S., P.B., E.B., L.P.; resources, Y.B., T.B., W.C., X.C., J.G., R.L., X.L. (Xiaozhen Liang), L.L., Z.Q., J.Q., D.S., Z.T., B.W., J.W., R.W., Z.W., M.X., L.Z., J.Z., S.D., G.M., J.M.M., V.F., M.A.V.F., C.P., V.V., S.B., L.B., M.B., N.F., P.P., E.V., M.A., V.B., G.Z., N.Z., X.L. (Xin Liu), X.B., Z.C., L.W., M.A.V.F. and J.M.M.; data curation, P.B., E.B., L.P.; writing—original draft preparation, P.B.; writing—review and editing, P.B. and N.M.; visualization, P.B. and L.P.; supervision, R.D.; project administration, O.A. and Y.D.; funding acquisition, N.M. All authors have read and agreed to the published version of the manuscript.

**Funding:** This research received no external funding.

**Institutional Review Board Statement:** Not applicable.

**Data Availability Statement:** Not applicable.

**Acknowledgments:** We would like to thanks all the HERD collaboration for its support and for making this experiment possible.

**Conflicts of Interest:** The authors declare no conflict of interest.

## References

1. HERD The High Energy Cosmic Radiation Detection Facility. Available online: <http://herd.ihep.ac.cn/> (accessed on 27 July 2022).
2. Pacini, L.; Adriani, O.; Bai, Y.I.; Bao, T.W.; Berti, E.; Bottai, S.; Cao, W.W.; Casaus, J.; Cui, X.Z.; D’Alessandro, R.; et al. Design and expected performances of the large acceptance calorimeter for the HERD space mission. In Proceedings of the 37th International Cosmic Ray Conference—PoS(ICRC2021), Berlin, Germany, 12–23 July 2021.
3. Berti, E.; Adriani, O.; Albergo, S.; Ambrosi, G.; Auditore, L.; Basti, A.; Bigongiari, G.; Bonechi, L.; Bonechi, S.; Bonghi, M.; et al. CaloCube: A new-concept calorimeter for the detection of high-energy cosmic rays in space. *Nucl. Instrum.* **2017**, *845*, 421–424. [[CrossRef](#)]
4. Adriani, O.; Albergo, S.; Auditore, L.; Basti, A.; Berti, E.; Bigongiari, G.; Bonechi, L.; Bonghi, M.; Bonvicini, V.; Bottai, S.; et al. Calocube—A highly segmented calorimeter for a space based experiment. *Nucl. Instrum.* **2016**, *824*, 609–613.
5. Bonghi, M.; Adriani, O.; Albergo, S.; Auditore, L.; Bagliesi, M.G.; Berti, E.; Bigongiari, G.; Boezio, M.; Bonechi, L.; Bonechi, S.; et al. CALOCUBE: An approach to high-granularity and homogeneous calorimetry for space based detectors. *J. Phys. Conf. Ser.* **2015**, *587*, 012029. [[CrossRef](#)]
6. Pacini, L.; Adriani, O.; Agnesi, A.; Albergo, S.; Auditore, L.; Basti, A.; Berti, E.; Bigongiari, G.; Bonechi, L.; Bonechi, S.; et al. CaloCube: An innovative homogeneous calorimeter for the next-generation space experiments. *J. Phys. Conf. Ser.* **2017**, *928*, 012013. [[CrossRef](#)]
7. Adriani, O.; Agnesi, A.; Albergo, S.; Antonelli, M.; Auditore, L.; Basti, A.; Berti, E.; Bigongiari, G.; Bonechi, L.; Bonghi, M.; et al. CaloCube: An isotropic spaceborne calorimeter for high-energy cosmic rays. Optimization of the detector performance for protons and nuclei. *Astropart. Phys.* **2017**, *96*, 11–17. [[CrossRef](#)]
8. Berti, E.; Adriani, O.; Albergo, S.; Ambrosi, G.; Auditore, L.; Basti, A.; Bigongiari, G.; Bonechi, L.; Bonechi, S.; Bonghi, M.; et al. CaloCube: A new concept calorimeter for the detection of high energy cosmic rays in space. *J. Phys. Conf. Ser.* **2019**, *1162*, 012042. [[CrossRef](#)]
9. Chang, J.; Ambrosi, G.; An, Q.; Asfiyarov, R.; Azzarello, P.; Bernardini, P.; Bertucci, B.; Cai, M.S.; Caragiulo, M.; Chen, D.Y.; et al. The DArk Matter Particle Explorer mission. *Astropart. Phys.* **2007**, *95*, 6–24. [[CrossRef](#)]

10. Bonvicini, V.; Orzan, G.; Zampa, G.; Zampa, N. A Double-Gain, Large Dynamic Range Front-end ASIC with A/D Conversion for Silicon Detectors Read-Out. *IEEE Trans. Nucl. Sci.* **2010**, *57*, 2963–2970. [[CrossRef](#)]
11. Chiari, M.; Barone, S.; Bombini, A.; Calzolari, G.; Carraresi, L.; Castelli, L.; Czelusniak, C.; Fedi, M.E.; Gelli, N.; Giambi, F.; et al. LABEC the INFN ion beam laboratory of nuclear techniques for environment and cultural heritage. *Eur. Phys. J. Plus* **2021**, *136*, 472. [[CrossRef](#)] [[PubMed](#)]